nature medicine

LETTERS

The *miR-15a–miR-16-1* cluster controls prostate cancer by targeting multiple oncogenic activities

Désirée Bonci[1], Valeria Coppola[1], Maria Musumeci[1], Antonio Addario[1], Raffaella Giuffrida[2], Lorenzo Memeo[2], Leonardo D'Urso[3], Alfredo Pagliuca[1], Mauro Biffoni[1], Catherine Labbaye[1], Monica Bartucci[1], Giovanni Muto[3], Cesare Peschle[1,4] & Ruggero De Maria[1,2]

MicroRNAs (miRNAs) are noncoding small RNAs that repress protein translation by targeting specific messenger RNAs. *miR-15a* and *miR-16-1* act as putative tumor suppressors by targeting the oncogene *BCL2*. These miRNAs form a cluster at the chromosomal region 13q14, which is frequently deleted in cancer. Here, we report that the *miR-15a* and *miR-16-1* cluster targets *CCND1* (encoding cyclin D1) and *WNT3A*, which promotes several tumorigenic features such as survival, proliferation and invasion. In cancer cells of advanced prostate tumors, the miR-15a and miR-16 level is significantly decreased, whereas the expression of BCL2, CCND1 and WNT3A is inversely upregulated. Delivery of antagomirs specific for miR-15a and miR-16 to normal mouse prostate results in marked hyperplasia, and knockdown of miR-15a and miR-16 promotes survival, proliferation and invasiveness of untransformed prostate cells, which become tumorigenic in immunodeficient NOD-SCID mice. Conversely, reconstitution of miR-15a and miR-16-1 expression results in growth arrest, apoptosis and marked regression of prostate tumor xenografts. Altogether, we propose that *miR-15a* and *miR-16* act as tumor suppressor genes in prostate cancer through the control of cell survival, proliferation and invasion. These findings have therapeutic implications and may be exploited for future treatment of prostate cancer.

Prostate cancer is the most common malignancy in men and one of the leading causes of cancer death[1]. Early-stage prostate cancer is curable, whereas more advanced tumors can be successfully treated only before tumor metastasis has occurred[2,3].

MiRNAs are small, noncoding, single-stranded RNAs of ~22 nucleotides that negatively regulate gene expression at the post-transcriptional level, primarily through base pairing to the 3′ untranslated region (UTR) of target mRNAs. Growing evidence indicates that miRNAs control basic cell functions, ranging from proliferation to apoptosis[4,5]. Although ~50% of miRNA genes are located in cancer-associated genomic regions or in fragile sites[6,7], few miRNAs have been proven to be directly involved in cancer development and progression[8]. *miR-15a* and *miR-16-1* are transcribed as a cluster (*miR-15a–miR-16-1*) that resides in the 13q14 chromosomal region. Deletions or point mutations in region 13q14 occur at high frequency in chronic lymphocytic leukemia, lymphoma and several solid tumors[6,9]. In prostate cancer, the frequency of allelic loss at 13q correlates with tumor progression, rising from 30% to 70% and 90% in early, advanced and metastatic tumors, respectively[10,11]. These observations suggest the existence of tumor suppressor gene(s) involved in prostate carcinogenesis within the 13q14 region[12].

We analyzed miR-15a and miR-16 expression in primary cells from 20 individuals with stage 2 or 3 prostate cancer (**Supplementary Table 1** and **Supplementary Fig. 1** online). Real-time PCR showed a consistent downregulation of both miR-15a and miR-16 in about 80% of the tumor samples with respect to their normal counterparts, particularly in more advanced tumors (**Fig. 1a** and **Supplementary Table 1**). *In situ* hybridization of 15 additional cases confirmed an overt decrease in the level of both miRNAs as compared to the normal tissue (**Fig. 1b** and **Supplementary Fig. 2** online). Although the gene encoding the tumor suppressor Rb is located 1.7 megabases upstream of *miR-15a–miR-16* in the 13q14 region[9,13], the analysis of several prostate samples did not show any correlation between Rb and miR-15a–miR-16 levels (**Supplementary Fig. 3** online), indicating that the loss of *miR-15a–miR-16* expression is often independent of the absence of the gene encoding Rb.

To explore the role of miRNA downregulation in the molecular mechanisms that regulate prostate cancer, we engineered a lentiviral vector named TWEEN 3′ UTR (TW3) with a multicloning site in the 3′ UTR[5,14] of an *EGFP* reporter gene, where we inserted two antisense sequences for miR-15a. Because miR-15a and miR-16 have a common seed sequence and share 80% complementarity, this vector, called TW 3′ UTR decoy miR-15a–miR-16 (decoy15-16 vector; **Supplementary Fig. 4a** online), encoded a stable transgene able to sequester and inhibit the activity of both miR-15a and miR-16 (**Supplementary Figs. 4** and **5**, **Supplementary Data** and **Supplementary Methods** online). The untransformed and growth factor–dependent prostate cell line

[1]Department of Hematology, Oncology and Molecular Medicine, Istituto Superiore Sanità, viale Regina Elena 299, 00161 Rome, Italy. [2]Department of Experimental Oncology, Mediterranean Institute of Oncology, via Penninazzo 7, 95029 Viagrande, Catania, Italy. [3]Department of Urology, San Giovanni Bosco Hospital, piazza Donatori del sangue 3, 10154 Turin, Italy. [4]Istituto di Ricovero e Cura a Carattere Scientifico, MultiMedica, via Fantoli 16/15, 20138 Milan, Italy. Correspondence should be addressed to R.D.M. (demaria@iss.it).

Received 19 June; accepted 22 September; published online 19 October 2008; doi:10.1038/nm.1880

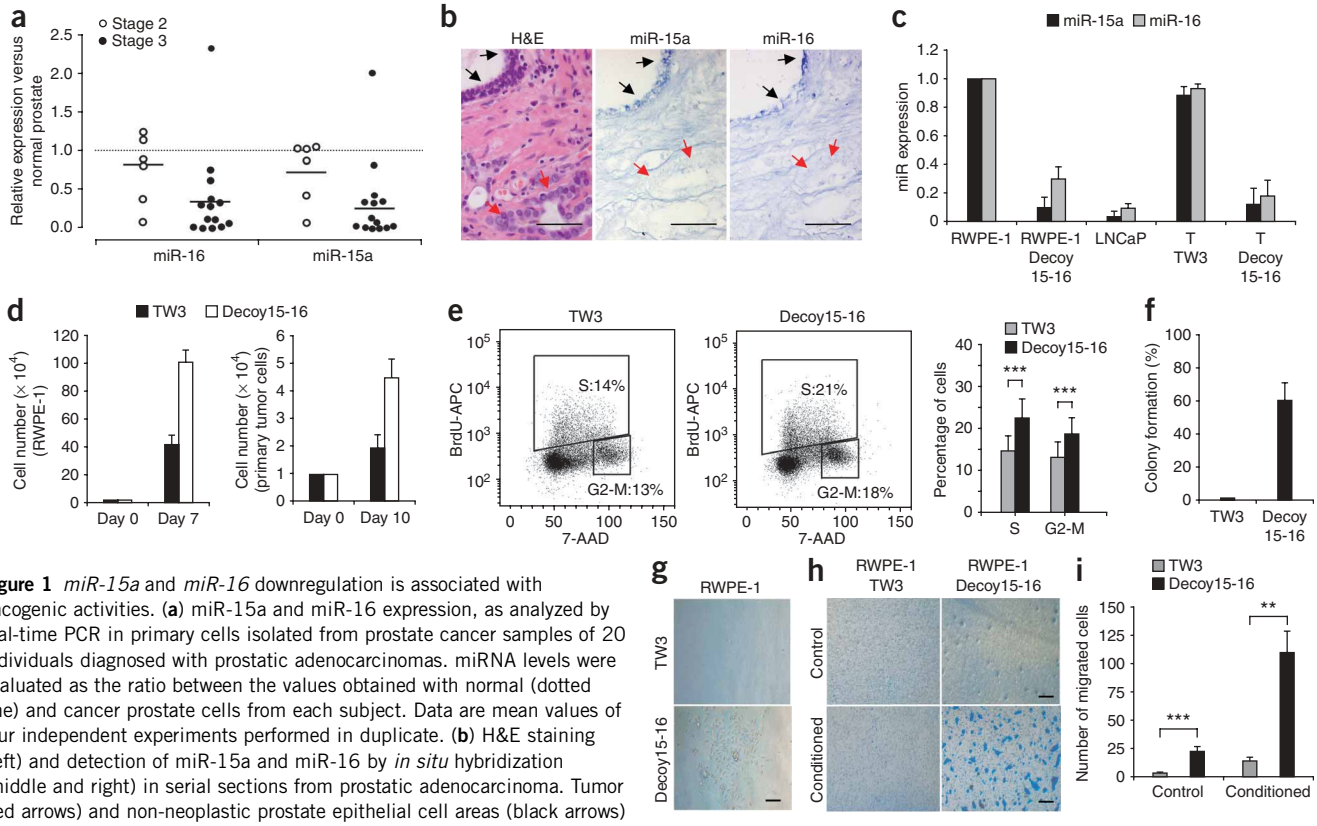

Figure 1 *miR-15a* and *miR-16* downregulation is associated with oncogenic activities. (**a**) miR-15a and miR-16 expression, as analyzed by real-time PCR in primary cells isolated from prostate cancer samples of 20 individuals diagnosed with prostatic adenocarcinomas. miRNA levels were evaluated as the ratio between the values obtained with normal (dotted line) and cancer prostate cells from each subject. Data are mean values of four independent experiments performed in duplicate. (**b**) H&E staining (left) and detection of miR-15a and miR-16 by *in situ* hybridization (middle and right) in serial sections from prostatic adenocarcinoma. Tumor (red arrows) and non-neoplastic prostate epithelial cell areas (black arrows) are indicated. Scale bars, 50 μm. (**c**) Real time PCR evaluation of miR-15a and miR-16 levels in wild-type or decoy15-16–transduced RWPE-1 cells, LNCaP cells, and primary tumor cells with normal levels of miR-15a and miR-16 (T) transduced with control (TW3) or decoy15-16 vectors. The untransformed prostate cell line RWPE-1 was used as expression reference. (**d**) Cell growth of RWPE-1 and primary tumor cells with normal miRNA expression transduced with decoy15-16 or the empty vector TW3. (**e**) Cell cycle analysis by cytofluorimetric profiling of BrdU-7AAD–stained RWPE-1 cells transduced with TW3 or decoy15-16 vector. $P < 0.001$ for the two groups. Data are means ± s.d. of five experiments evaluating the relative percentage of cells at S and G2/M phase of the cell cycle. (**f**,**g**) Soft agar colony formation assay for RWPE-1 cells transduced with TW3 or decoy15-16. Data are means ± s.d. of three independent experiments. (**h**,**i**) Migration assay for RWPE-1 cells transduced with TW3 or decoy15-16 and maintained in standard culture medium (Control) or in prostate cancer fibroblast–conditioned medium (Conditioned). $^{**}P < 0.01$ and $^{***}P < 0.001$. Data are means ± s.d. of four independent experiments in **c**,**d** and **i**. Scale bars, 100 μm.

RWPE-1 (ref. 24) and primary tumor prostate cells with normal miR-15 and miR-16 levels were infected with decoy15-16 virus. Shortly after transduction, we observed a considerable decrease of both miR-15a and miR-16 in decoy15-16–infected cells (**Fig. 1c** and **Supplementary Fig. 5b**). Levels of miR-15a and miR-16 in decoy15-16 infected cells were only slightly higher than those detected in the 13q14-defective LNCaP prostate cancer cell line[15]. Both RWPE-1 and primary tumor prostate cells transduced with decoy15-16 showed a considerable increase in proliferation, as assessed by cell number and cell cycle analysis (**Fig. 1d**,**e**). Unlike wild-type and control vector-transduced cells, RWPE-1 cells infected with decoy15-16 vector were able to grow in agar, giving rise to colonies that showed anchorage-independent growth (**Fig. 1f**,**g**). Moreover, RWPE-1 cells infected with decoy15-16 revealed intrinsic migration capacity in standard medium and enhanced invasion and motility in cancer fibroblast-conditioned medium (**Fig. 1h**,**i**). These data establish a direct correlation between miRNA silencing and increased proliferation and migration.

To determine the consequence of miR-15a–miR-16 restoration in prostate cancer cells, we subcloned the *miR-15a–miR-16-1* genomic cluster into the TWEEN lentiviral vector[16–18] (TWmiR-15-16 vector; **Fig. 2a**). We then transduced LNCaP and miR-15– and miR-16–defective primary tumor cells with TWmiR-15-16 vector to obtain a near-physiological expression level of both miRNAs (**Fig. 2**). The RWPE-1 and normal primary cells were infected in parallel (**Fig. 2d**,**g**) to investigate the possible toxicity deriving from miR-15a and miR-16 overexpression. Reconstitution of miR-15a and miR-16 in LNCaP and primary tumor cells resulted in growth arrest and apoptosis, whereas exogenous expression of miR-15a and miR-16 in RWPE-1 and normal primary cells did not induce any sign of toxicity (**Fig. 2c–g**). After gene transfer, the few surviving TWmiR-15-16–infected LNCaP cells underwent massive counterselection that was not observed in control vector–infected LNCaP cells (**Fig. 2e**), suggesting that loss of miR-15a and miR-16 creates addiction in transformed cells.

Docetaxel is the standard treatment for androgen-independent prostate tumors[3]. We found that sensitivity to docetaxel was clearly dependent on miR-15a and miR-16 expression (**Supplementary Fig. 6** online). Thus, reconstitution of *miR-15a–miR-16* in defective prostate cancer cells induces a considerable cytotoxic effect that is further increased by chemotherapy.

To identify new targets of miR-15a and miR-16, we ran a computer-assisted search that generated a list of >400 potential targets, which we refined by applying increasing stringency in the selection criteria (see Methods for details). Among the possible candidates, we further analyzed *CCND1*, *WNT3A* and *PIM1*, three genes whose functions are directly associated with cancer progression and invasion[19–21]. *CCND1*

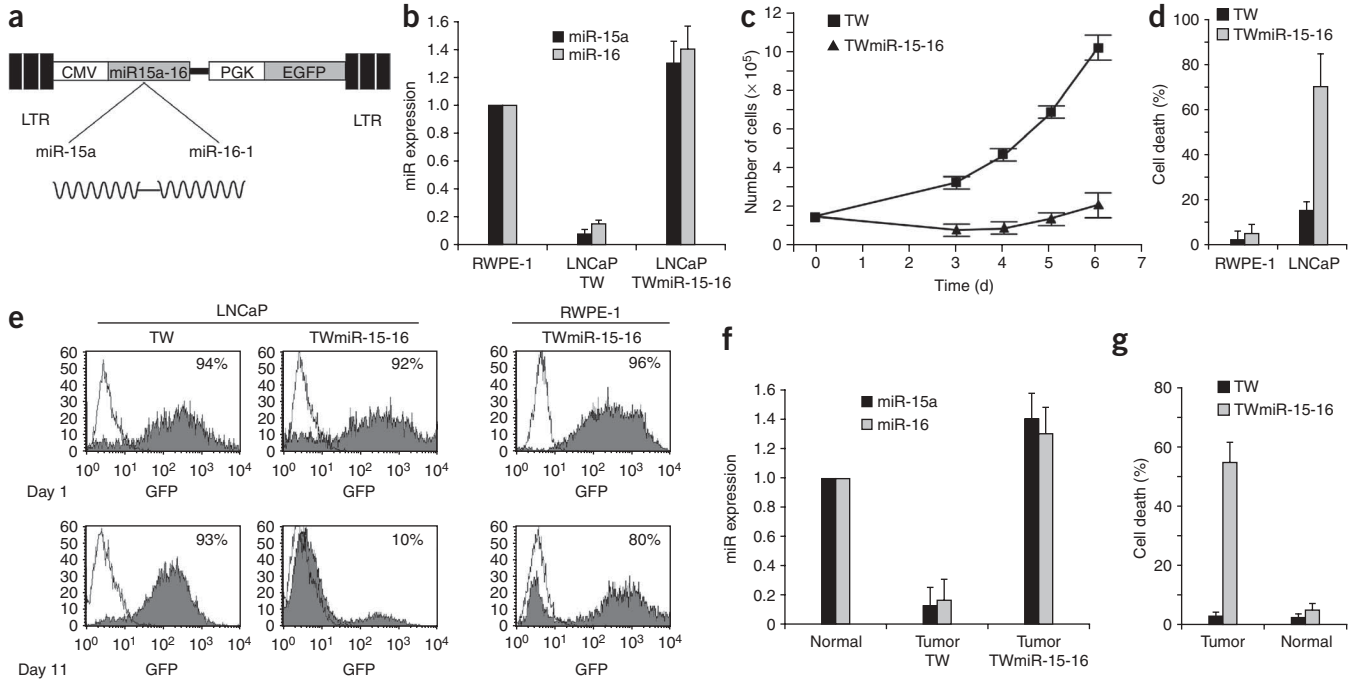

Figure 2 Restoration of miR-15a and miR-16 induces growth arrest and apoptosis in defective prostate cancer cells. (**a**) Schematic depiction of TWmiR-15-16. The *miR-15a-miR-16-1* cluster was subcloned in the TWEEN vector under the control of the cytomegalovirus (CMV) promoter. PGK, phosphoglycerate kinase promoter. (**b**) Real-time PCR evaluation of miR-15a and miR-16 expression in LNCaP cells transduced with TWmiR-15-16 vector. Transduced cells were compared with cells infected with empty vector (TW) and with the RWPE-1 cell line. (**c**) Cell growth of LNCaP cells infected with empty vector (TW) or TWmiR-15-16. Data are means ± s.d. of four independent experiments. (**d**) Cell death of normal (RWPE-1) and tumor (LNCaP) cells transduced with TWmiR-15-16 or control vector, as evaluated 48 h after lentiviral infection. (**e**) Flow cytometry profiles of LNCaP and RWPE-1 cells infected with TW and TWmiR-15-16 viruses. GFP expression is shown 24 h (Day 1) and 11 d after infection. The percentages represent GFP-positive cells. (**f**) Real-time PCR analysis of miR-15a and miR-16 expression in miR-15– and miR-16–defective prostate tumor primary cells after transduction with TWmiR-15-16 or empty TW vector. Primary normal prostate cells were used as expression reference. (**g**) Cell death evaluation in tumor and normal prostate primary cells infected as in **f**. Data are means ± s.d. of three independent experiments for all panels except **c**.

and *WNT3A* showed a particularly high prediction ranking, whereas *PIM1* showed a higher estimated false discovery rate (**Supplementary Table 2** online). A luciferase assay performed by cotransfecting pGL3–3′ UTR vectors along with synthetic miR-15a or miR-16 indicated a direct interaction of both miRNAs with *CCND1* and *WNT3A* 3′ UTRs to the same extent as that measured for *BCL2*, whereas the *PIM1* 3′ UTR was confirmed as a nontargeted region (**Fig. 3a**, **Supplementary Fig. 7** and **Supplementary Methods** online). Immunoblot analysis supported the data obtained with the reporter gene assays for *BCL2*, *WNT3A* and *CCND1* (**Fig. 3b**,**c** and **Supplementary Fig. 8a–d** online). We then analyzed miR-15a– and miR-16–defective prostate tumors for expression of BCL2, CCND1 and WNT3A. Immunohistochemical and immunoblot analysis showed a significant ($P = 0.008$) inverse correlation between miR-15a–miR-16 expression and target protein amounts (**Fig. 3d**,**e**).

WNT3A signaling promotes increased β-catenin protein abundance and the activation of other survival and proliferation pathways through the phosphorylation of the kinases ERK and Akt[22,23]. Accordingly, the presence of miR-15a and miR-16 was associated with a decreased expression of β-catenin and a reduced phosphorylation of AKT and ERK (**Fig. 3f** and **Supplementary Fig. 8e**). Moreover, the increased expression of CCND1 in RWPE-1 cells infected with decoy15-16 correlated with an increased phosphorylation of Rb, whereas the exogenous expression of miR-15a–miR-16 in LNCaP cells produced the opposite effect (**Fig. 3f** and **Supplementary Fig. 8e**). Thus, miR-15a and miR-16 inhibit prostate cell survival, proliferation and invasion through the targeting of *BCL2*, *CCND1* and *WNT3A*. Exogenous gene delivery showed that *CCND1* and *WNT3A* increase prostate cell proliferation (**Supplementary Fig. 9a**,**b** online); WNT3A promotes the invasion and motility of RWPE-1 cells (**Supplementary Fig. 9c**), whereas BCL2 and WNT3A synergistically counteract the cytotoxic activity of docetaxel (**Supplementary Fig. 10** online), suggesting that these targets may act in concert in prostate cancer after the loss of miR-15a and miR-16.

We next investigated whether the loss of function of *miR-15a* and *miR-16* would endow the nontumorigenic cell line RWPE-1 with the ability to form tumors in NOD-SCID mice. RWPE-1 cells infected with decoy15-16 were able to consistently produce slow-growing tumors in 4-week-old male mice, whereas RWPE-1 cells expressing empty TW3 vector never developed into a tumoral mass (**Fig. 4a**). To determine the possible cooperation with another oncogenic lesion, we devised a similar experiment with RWPE-1 cells transformed with ki-RAS (RWPE-2 cells)[24]. Upon injection into NOD-SCID mice, RWPE-2 cells infected with decoy15-16 produced tumors with a considerably increased volume as compared with control RWPE-2 cells (**Fig. 4b**). To demonstrate that the decreased expression of miR-15 and miR-16 promotes prostate cell invasiveness *in vivo*, we injected NOD-SCID mice subcutaneously with a combination of wild-type (70%) and decoy15-16–transduced (30%) RWPE-1 cells. After tumor formation, we analyzed the localization of decoy15-16–transduced cells by immunohistochemistry through staining of the GFP reporter, which

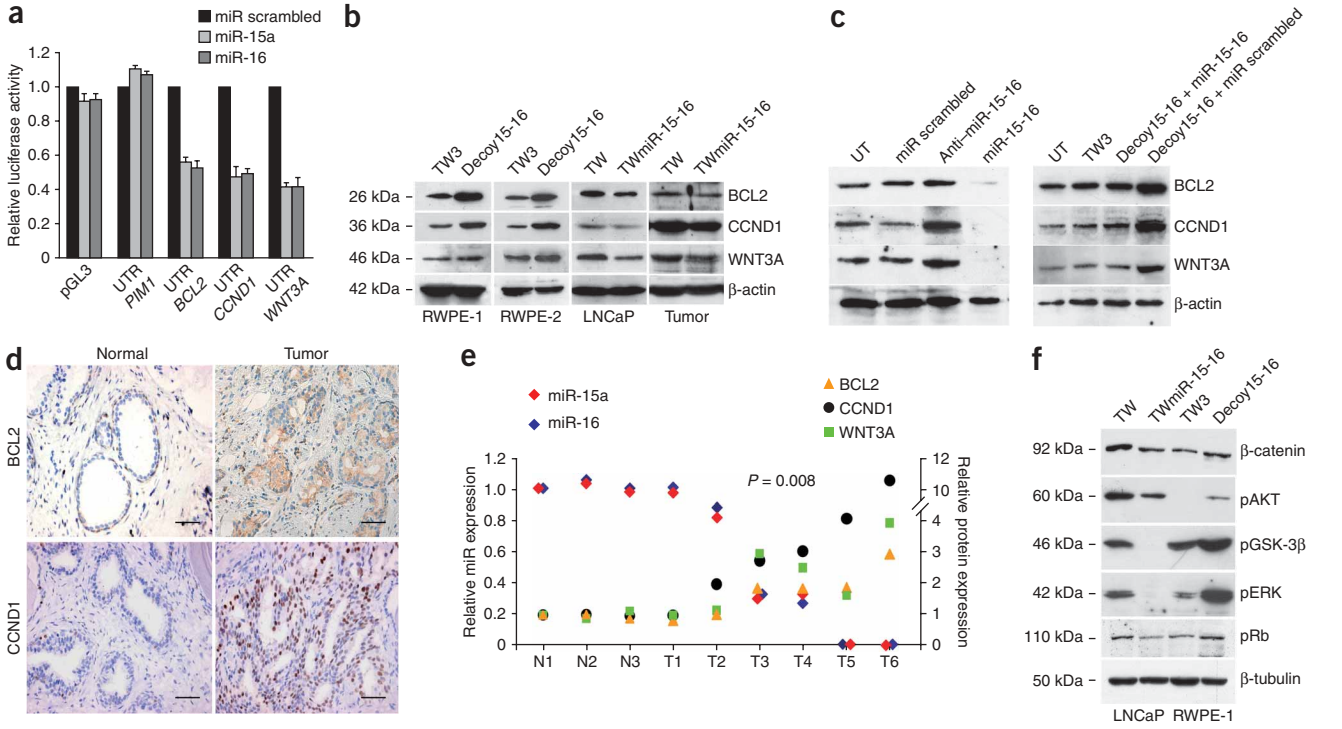

Figure 3 miR-15a and miR-16 target *CCND1* and *WNT3A*. (**a**) Luciferase activity 48 h after cotransfection of K562 cells with pGL3 and pGL3-UTRs vectors and miR-15a, miR-16 or miR-scrambled oligonucleotides. Data are means ± s.d. of five independent experiments. (**b**) Western blot analysis of *miR-15a–miR-16* targets in RWPE-1, RWPE-2, LNCaP and miR-defective tumoral primary cells (Tumor) transduced with either decoy15-16 or TWmiR-15-16 and the corresponding control vectors. (**c**) Western blot analysis of BCL2, CCND1 and WNT3A expression in wild-type RWPE-1 cells untreated (UT) or treated with scrambled, miR-15–miR-16 antisense (antimiR-15-16) or sense (miR-15-16) oligonucleotides (left), and wild-type (UT), TW3-transduced and decoy15-16–transduced RWPE-1 cells treated for 48 h with miR-15-16 or miR-scrambled oligonucleotides (right). β-actin levels were used as loading control. One representative experiment of three is shown. (**d**) BCL2 and CCND1 immunohistochemical staining of normal prostate tissue and miR-15–miR-16–defective tumors. One representative case of three nontumoral controls and five miR-15–miR-16 defective tumors is shown. Scale bars, 50 μm. (**e**) Inverse correlation between miR-15a and miR-16 and target proteins in primary prostate cultures. The miRNA expression was evaluated by real-time PCR, normalizing over a normal sample (N1) used as expression reference. Protein abundance was reported as western blotting densitometry normalized to β-actin protein expression and then compared to N1. Nine indicative samples are shown. A correlation coefficient of –0.81 with a $P = 0.008$ indicates an inverse relationship between miR-15 and miR-16 expression and the levels of CCND1, BCL2 and WNT3A. (**f**) Western blot analysis of β-catenin, phosphorylated AKT (pAKT), phosphorylated glycogen synthase kinase-3β (pGSK-3β), phosphorylated ERK (pERK) and phosphorylated Rb (pRb) in LNCaP and RWPE-1 cells transduced as indicated. One representative of three independent experiments is shown.

was absent in wild-type RWPE-1 cells. Such analysis revealed that miR-15a and miR-16 downregulation enhances prostate cell invasion, as indicated by the presence of GFP-expressing cells in the tumor front and in invasive tumor islands, whereas GFP-negative cells were not located in such areas (**Fig. 4c**). Hence, miR-15a–miR-16 downregulation can contribute to prostate cancer transformation and invasiveness.

Antagomir oligonucleotides can efficiently knock down specific miRNAs *in vivo* for as long as 1 month after injection[5,25]. To investigate the role of miR-15a and miR-16 downregulation *in vivo*, we injected BALB/c mouse prostates with a single dose of mixed antagomirs selective for miR-15a and miR-16 (antagomir–15-16). As controls, mice were injected with either saline buffer or the cardio-specific antagomir-1. Inhibition by antagomir–15-16 was evaluated by real-time PCR one week to one month after injection, resulting in about 40–85% repression of endogenous miR-15a and miR-16 compared to control mice (**Supplementary Fig. 11a,b** online). In line with the potential tumor suppressor role of *miR-15a–miR-16-1*, histological analysis showed a marked prostatic hyperplasia and a modest acini disruption in antagomir–15-16–treated mice, whereas control mice did not show any alteration (**Fig. 4d**). Immunohistochemical and immunoblot analyses of antagomir–15-16–treated prostates showed a considerable upregulation of Ccnd1 and Wnt3a, whereas Bcl2 was not upregulated in hyperplastic tissues (**Supplementary Fig. 11c,d**). These data confirm that CCND1 and WNT3A are targets of miR-15a and miR-16, and that such miRNAs are key tumor suppressor genes that control prostate cancer development.

To evaluate the effect of restored miR-15a and miR-16 expression *in vivo*, we injected LNCaP-derived tumors with TWmiR-15-16 or TW control viruses (**Supplementary Fig. 11e**). TWmiR-15-16–treated tumors underwent growth arrest within 1 week of treatment and considerable volume regression thereafter, whereas similar tumors did not alter their growth after injection with empty-vector virus (**Fig. 4e**). The antitumor effect of miR-15a–miR-16 treatment was particularly potent, as the histological analysis of the residual masses indicated the presence of diffuse necrosis with rare areas containing surviving cells (**Fig. 4f**). Thus, in line with the *in vitro* observations, restoration of miR-15a and miR-16 expression in prostate cancer cells resulted in dramatic tumor regression.

Here we have demonstrated that miR-15a and miR-16 are down-regulated in two of six stage 2 and twelve of fourteen stage 3 prostate

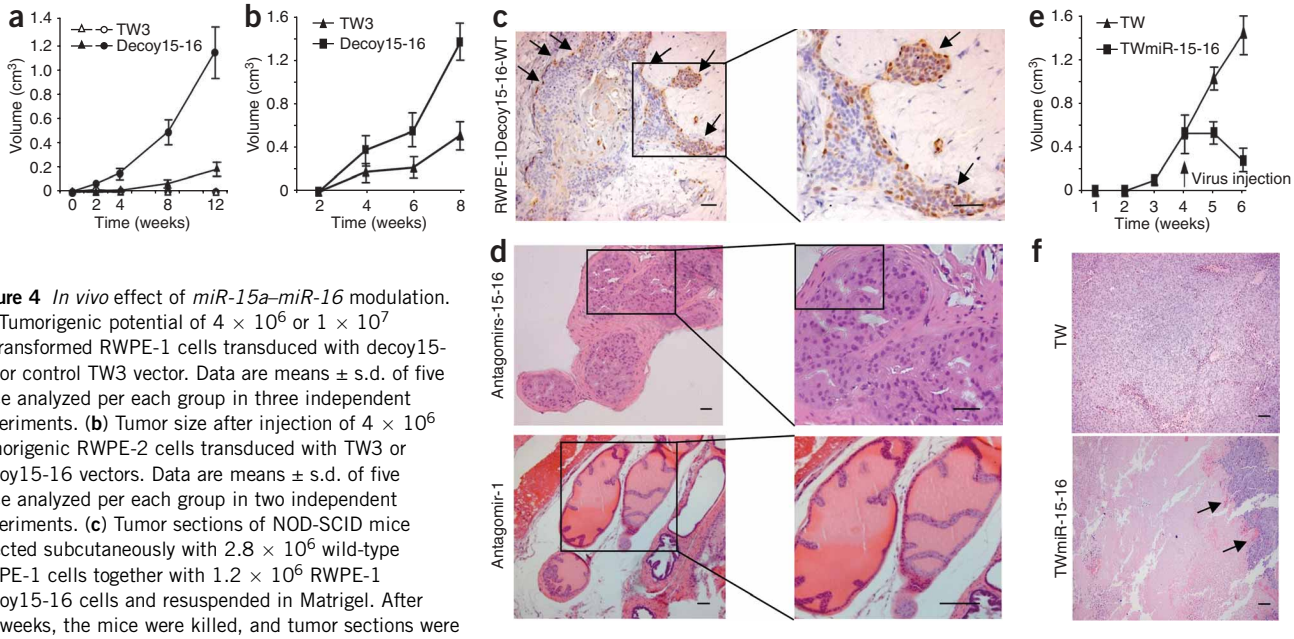

Figure 4 *In vivo* effect of *miR-15a–miR-16* modulation. (**a**) Tumorigenic potential of 4×10^6 or 1×10^7 untransformed RWPE-1 cells transduced with decoy15-16 or control TW3 vector. Data are means ± s.d. of five mice analyzed per each group in three independent experiments. (**b**) Tumor size after injection of 4×10^6 tumorigenic RWPE-2 cells transduced with TW3 or decoy15-16 vectors. Data are means ± s.d. of five mice analyzed per each group in two independent experiments. (**c**) Tumor sections of NOD-SCID mice injected subcutaneously with 2.8×10^6 wild-type RWPE-1 cells together with 1.2×10^6 RWPE-1 decoy15-16 cells and resuspended in Matrigel. After 12 weeks, the mice were killed, and tumor sections were stained with antibody to GFP. Arrows indicate GFP^+ cells at the tumor front. Six mice were analyzed in two independent experiments. (**d**) H&E staining of mouse prostates after five weeks from local injection of either a combination of antagomir-15 and antagomir-16 (antagomir–15-16) or antagomir-1 as a control. Five mice per each group were analyzed in two independent experiments. (**e**) Effect on tumor growth of *miR-15a-miR-16* reconstitution. Tumors generated four weeks after injection of 8×10^6 LNCaP cells were treated with virus particles containing TW and TWmiR-15-16 vectors. Data are means ± s.d. of three independent experiments with three mice per each group. (**f**) H&E staining of six-week LNCaP xenografts, two weeks after injection of TW or TWmiR-15-16 viral particles. Rare living tumor cell islands in a necrotic tumor treated with TWmiR-15-16 vector are indicated by arrows. Scale bars, 50 μm.

tumors studied. *In vitro* and *in vivo* knockdown of miR-15a and miR-16 enhances prostate cancer progression while promoting cell growth, survival and invasion. Both miRNAs are able to target *BCL2*, *CCND1* and *WNT3A*, whose protein levels are consequently upregulated and may synergistically contribute to potentiate tumor cell survival, proliferation and invasion.

The *miR-15a–miR-16* cluster is usually deleted in advanced prostate cancer. However, a small fraction of early prostate tumors show deletion of the 13q14 region[10,11], suggesting that in some rare instances the loss of miR-15a–miR-16 might occur during the initial stages of tumor development.

We showed that *in vivo* knockdown of miR-15a–miR-16 results in prostate hyperplasia with disruption of glandular acini associated with Ccnd1 and Wnt3a upregulation, indicating that loss of miR-15a–miR-16 could be a relevant pathogenic event even in the early phases of tumorigenic process and in the absence of Bcl2. After the loss of miR-15a and miR-16 in tumor lesions, larger amounts of BCL2 and WNT3A may enhance prostate cell growth by inhibiting apoptosis in unfavorable conditions, as in the case of antiandrogen or cytotoxic therapies. Both CCND1 and WNT3A are able to promote the proliferation of prostate cells upon silencing of miR-15a and miR-16, whereas the single increase in WNT3A expression seems responsible for the enhanced migration and invasiveness typical of advanced tumor stages. Although BCL2, CCND1 and WNT3A seem to have a key role in prostate cancer progression driven by the loss of miR-15–miR-16, there are hundreds of predicted targets for single miRNAs. Therefore it is very likely that this miRNA cluster can target a number of other oncogenes relevant for prostate cancer.

Our data may have therapeutic significance for prostate cancer. Ongoing clinical trials are assessing the therapeutic potential of antisense oligonucleotides targeting *BCL2* gene expression in prostate cancer[26]. The reintroduction of *miR-15a–miR-16* could be theoretically more effective, due to the simultaneous inhibition of *BCL2, CCND1, WNT3A* and other possible targets involved in cancer cell proliferation and resistance to apoptosis. In our experimental models, delivery of miR-15a and miR-16 to prostate cancer xenografts was able to induce a marked tumor regression. In this study the cytotoxic effect of these miRNAs on both LNCaP and primary prostate tumor cells was noteworthy and was further increased in the presence of docetaxel. Thus, although prostate tumors are extremely heterogeneous in the clinical setting, miR-15a and miR-16 may have considerable therapeutic potential, both as single agents or in combination with chemotherapeutic drugs.

The field of small RNAs is rapidly advancing toward *in vivo* delivery for therapeutic purposes. Advanced molecular therapies aimed at downmodulating the level of a given miRNA in model organisms have been successfully established[5,25]. Likewise, siRNA technologies allow effective introduction of artificial RNA guide strands in the RNA-induced signaling complex in primates[27]. We thus envision that similar strategies may be exploited to restore *miR-15a–miR-16* function for prostate cancer therapy.

METHODS

Tissue and cell assays. We obtained LNCaP, RWPE-1 and RWPE-2 cell lines from American Type Culture Collection and cultivated them in the recommended media. We obtained tissue samples from radical prostatectomies at the Department of Urology, San Giovanni Bosco Hospital of Turin. All samples were collected with the informed consent of the patients and the study was approved by the Ethics Committee of Istituto Superiore di Sanità (Prot. PRE 2002/06, Rif. CE-ISS 06/140). The study was also performed according to protocols approved by the Istituto Superiore di Sanità Committee. We performed tissue dissociation and isolation of primary prostate cells as previously described[28] with some modifications (**Supplementary Methods**

online). We cultured tumoral and nontumoral prostate surgical specimens in collagen-coated plates with BRFF-HPC1 (biological research faculty and facility–human prostate cell 1) medium (AthenaES). We confirmed the purity of human prostate primary cell preparations by immunocytochemistry and FACS analysis through the absence of the stromal marker Thy-1 and the expression of epithelial cell–specific cytokeratins (CK18/8; >85% purity). For the soft-agar assay, we resuspended RWPE-1 cells infected with TW3 vector or decoy15-16 in culture medium supplemented with 0.4% agar and plated them at a density of 100, 250, 500 cells per well in duplicate in a 24-well plate previously coated with a 3-mm layer of the same modified medium. We cultured cells for two weeks before the analysis. We performed three separate experiments for each cellular density. We tested chemotaxis in modified Boyden chambers containing porous (8-μm), uncoated, polycarbonate membranes (Corning Incorporated). Details are in the **Supplementary Methods**.

Generation of lentiviral vectors and gene transfer. For TWmiR-15-16 generation, we PCR-amplified *miR-15a–miR-16-1* precursor DNA from human genomic DNA. We subcloned the amplified fragment spanning 724 base pairs (NCBI36: ch13:49519256:49523338 genomic region) into the lentiviral vector TWEEN[17] under control of the cytomegalovirus promoter. We confirmed miRNA transgene expression by real-time PCR with the appropriate assay from Applied Biosystems. We engineered the TW3 vector by modifying the *EGFP* 3′ UTR of the TWEEN vector through the insertion of a multicloning site (*Xho*I-*Xba*I) that allowed the subcloning of antisense miR sequences. Then we inserted the modified 3′ UTR cassette under control of the cytomegalovirus promoter. Moreover, we inserted a puromycin resistance gene under control of the phosphoglycerate kinase promoter to allow the selection of transduced cells (**Supplementary Methods** and **Supplementary Data**). We obtained recombinant lentiviral particles as previously described[16]. We infected cells with 1×10^6 viral transducing units per ml, as previously indicated[16]. For *in vivo* experiments, we concentrated the viral supernatant 250-fold. To obtain high-titer vector stocks, we ultracentrifuged the virus and injected it in 200 μl of PBS directly into tumor xenografts of NOD-SCID mice (**Supplementary Methods**).

***In vivo* assay.** We used six–eight-week-old male NOD-SCID mice (Charles River Laboratory) for examining the tumorigenicity of decoy15-16–infected RWPE-1 and decoy15-16–infected RWPE-2 cells and for evaluation of cytotoxic activity of miR-15 and miR-16 in LNCaP xenografts. For antagomir delivery, we gave six-week-old male BALB/c mice a single dose of mixed antagomir selective for miR-15a and miR-16 by intraprostatic injection through a transverse incision in the lower abdomen. We used saline buffer and the unrelated cardio-specific antagomir targeting miR-1 as controls (**Supplementary Methods**). All animal procedures were performed according to protocols approved by the Istituto Superiore di Sanità Animal Care Committee.

***In situ* hybridization and immunohistochemistry.** We used locked nucleic acid–modified probes biotinylated at the 5′ end (Exiqon) to detect the *in situ* hybridization signal for miR-15a and miR-16 on formalin-fixed, paraffin-embedded prostate tissue. We performed *in situ* hybridization as previously described[29] with some modifications (**Supplementary Methods**). We performed immunohistochemistry experiments on 2-μm–thick formalin-fixed, paraffin-embedded tissue slices. After dewaxing, we permeabilized sections for 30 min with Tris-buffered saline (TBS) containing 0.4% Triton X-100 and then blocked them for 30 min with TBS containing 5% BSA. We then incubated the sections overnight at 4 °C with the primary antibodies. Mouse antibody to BCL2 (1 to 100 dilution) was from BioGenex, mouse antibody to CCND1 (1 to 20) was from Dako and rabbit antibody to EGFP (1 to 200) was from Invitrogen. For mouse tissue experiments, we used rabbit antibody to Ccnd1 (1 to 100) and rabbit antibody to Bcl2 (1 to 200) from Novus Biologicals. After washing the sections with TBS, we incubated them for 1 h at 22 °C with biotinylated secondary antibody to mouse or rabbit (1 to 500, Jackson Laboratories) and treated them with streptavidin conjugated to horseradish peroxidase (Dako). Finally, we detected the signal with diaminobenzidine as chromogen. We counterstained sections with hematoxylin, dehydrated them and mounted them with xylene.

Reporter assays. We amplified the 3′ UTR segments of *BCL2*, *CCND1* and *WNT3A* by PCR from normal human genomic DNA and subcloned them into the 3′ UTR of the firefly luciferase coding sequence into pGL3-Promoter (Promega; **Supplementary Methods**).

Target screening. In this study, we used three publicly available search engines for target prediction: TargetScan (Release 2.1), http://genes.mit.edu/targetscan (refs. 4,30,31) miRanda, http://www.microrna.org (ref. 32) and PicTar, http://pictar.bio.nyu.edu (ref. 33). We obtained the putative targets common to the different algorithms by sequentially inputting TargetScan hits into PicTar and then into Miranda. The *P* value for any target in this list was computed by TargetScan, and a threshold value of <0.1 was set for positive selection. This procedure yielded a list of 61 top-scoring candidates, of which only a few could directly promote cell proliferation.

Western and northern blotting, RNA extraction and quantitative real-time PCR. Please see the **Supplementary Methods**.

Statistical analyses. Data are presented as the means ± s.d. We analyzed the results of BrdU assays by two-way analysis of variance and Bonferroni post-tests. We analyzed the migration assay with Student's *t*-test. We performed the Spearman correlation analysis between miRNAs and their corresponding targets.

Note: Supplementary information is available on the Nature Medicine website.

ACKNOWLEDGMENTS

We thank G. Loreto, A. Di Virgilio and M. Blasi for technical assistance and E. Palio and M. Gulisano for valuable discussion and suggestions. This work was supported by the Italian Health Ministry, the Italian Ministry of University and Research (project number RBIP06ZJ78), and the Italian Association for Cancer Research. M. Bartucci is a recipient of a fellowship from the Italian Association for Cancer Research.

AUTHOR CONTRIBUTIONS

D.B., V.C., M.M., A.A., R.G., L.M., L.D., A.P., M. Biffoni, C.L. and M. Bartucci conducted the *in vitro* and *in vivo* experiments. G.M., D.B. and R.D.M. planned the experiments. L.D. provided human samples. G.M. and C.P. discussed the results and commented on the manuscript. R.D.M. wrote the manuscript and was responsible for research coordination and strategy.

Published online at http://www.nature.com/naturemedicine/
Reprints and permissions information is available online at http://npg.nature.com/reprintsandpermissions/

1. Jemal, A. *et al.* Cancer statistics, 2006. *CA Cancer J. Clin.* **56**, 106–130 (2006).
2. Loberg, R.D., Logothetis, C.J., Keller, E.T. & Pienta, K.J. Pathogenesis and treatment of prostate cancer bone metastases: targeting the lethal phenotype. *J. Clin. Oncol.* **23**, 8232–8241 (2005).
3. Pienta, K.J. & Smith, D.C. Advances in prostate cancer chemotherapy: a new era begins. *CA Cancer J. Clin.* **55**, 300–318 (2005).
4. Bartel, D.P. MicroRNAs: genomics, biogenesis, mechanism, and function. *Cell* **116**, 281–297 (2004).
5. Care, A. *et al.* MicroRNA-133 controls cardiac hypertrophy. *Nat. Med.* **13**, 613–618 (2007).
6. Calin, G.A. *et al.* A MicroRNA signature associated with prognosis and progression in chronic lymphocytic leukemia. *N. Engl. J. Med.* **353**, 1793–1801 (2005).
7. Calin, G.A. *et al.* Human microRNA genes are frequently located at fragile sites and genomic regions involved in cancers. *Proc. Natl. Acad. Sci. USA* **101**, 2999–3004 (2004).
8. Esquela-Kerscher, A. & Slack, F.J. Oncomirs—microRNAs with a role in cancer. *Nat. Rev. Cancer* **6**, 259–269 (2006).
9. Calin, G.A. *et al.* Frequent deletions and down-regulation of micro-RNA genes miR15 and miR16 at 13q14 in chronic lymphocytic leukemia. *Proc. Natl. Acad. Sci. USA* **99**, 15524–15529 (2002).
10. Dong, J.T., Boyd, J.C. & Frierson, H.F. Jr. Loss of heterozygosity at 13q14 and 13q21 in high-grade, high-stage prostate cancer. *Prostate* **49**, 166–171 (2001).
11. Hyytinen, E.R., Frierson, H.F., Jr., Boyd, J.C., Chung, L.W. & Dong, J.T. Three distinct regions of allelic loss at 13q14, 13q21–22, and 13q33 in prostate cancer. *Genes Chromosom. Cancer* **25**, 108–114 (1999).
12. Cimmino, A. *et al.* miR-15 and miR-16 induce apoptosis by targeting BCL2. *Proc. Natl. Acad. Sci. USA* **102**, 13944–13949 (2005).
13. Yin, Z. *et al.* Limiting the location of a putative human prostate cancer tumor suppressor gene at chromosome 13q14.3. *Oncogene* **18**, 7576–7583 (1999).
14. Ebert, M.S., Neilson, J.R. & Sharp, P.A. MicroRNA sponges: competitive inhibitors of small RNAs in mammalian cells. *Nat. Methods* **4**, 721–726 (2007).
15. Nupponen, N.N., Hyytinen, E.R., Kallioniemi, A.H. & Visakorpi, T. Genetic alterations in prostate cancer cell lines detected by comparative genomic hybridization. *Cancer Genet. Cytogenet.* **101**, 53–57 (1998).

16. Bonci, D. *et al.* 'Advanced' generation lentiviruses as efficient vectors for cardiomyocyte gene transduction *in vitro* and *in vivo*. *Gene Ther.* **10**, 630–636 (2003).
17. Felli, N. *et al.* MicroRNAs 221 and 222 inhibit normal erythropoiesis and erythroleukemic cell growth via kit receptor down-modulation. *Proc. Natl. Acad. Sci. USA* **102**, 18081–18086 (2005).
18. Follenzi, A., Ailles, L.E., Bakovic, S., Geuna, M. & Naldini, L. Gene transfer by lentiviral vectors is limited by nuclear translocation and rescued by HIV-1 pol sequences. *Nat. Genet.* **25**, 217–222 (2000).
19. Clevers, H. Wnt/β-catenin signaling in development and disease. *Cell* **127**, 469–480 (2006).
20. Dhanasekaran, S.M. *et al.* Delineation of prognostic biomarkers in prostate cancer. *Nature* **412**, 822–826 (2001).
21. Sherr, C.J. Cancer cell cycles. *Science* **274**, 1672–1677 (1996).
22. Almeida, M., Han, L., Bellido, T., Manolagas, S.C. & Kousteni, S. Wnt proteins prevent apoptosis of both uncommitted osteoblast progenitors and differentiated osteoblasts by β-catenin–dependent and –independent signaling cascades involving Src/ERK and phosphatidylinositol 3-kinase/AKT. *J. Biol. Chem.* **280**, 41342–41351 (2005).
23. Yun, M.S., Kim, S.E., Jeon, S.H., Lee, J.S. & Choi, K.Y. Both ERK and Wnt/β-catenin pathways are involved in WNT3A-induced proliferation. *J. Cell Sci.* **118**, 313–322 (2005).
24. Bello, D., Webber, M.M., Kleinman, H.K., Wartinger, D.D. & Rhim, J.S. Androgen responsive adult human prostatic epithelial cell lines immortalized by human papillomavirus 18. *Carcinogenesis* **18**, 1215–1223 (1997).
25. Krutzfeldt, J. *et al.* Silencing of microRNAs *in vivo* with 'antagomirs'. *Nature* **438**, 685–689 (2005).
26. Tolcher, A.W. *et al.* A phase II, pharmacokinetic, and biological correlative study of oblimersen sodium and docetaxel in patients with hormone-refractory prostate cancer. *Clin. Cancer Res.* **11**, 3854–3861 (2005).
27. Zimmermann, T.S. *et al.* RNAi-mediated gene silencing in non-human primates. *Nature* **441**, 111–114 (2006).
28. Navone, N.M., Olive, M. & Troncoso, P. Isolation and culture of prostate cancer cell lines. *Methods Mol. Med.* **88**, 121–132 (2004).
29. Nelson, P.T. *et al.* RAKE and LNA-ISH reveal microRNA expression and localization in archival human brain. *RNA* **12**, 187–191 (2006).
30. Lewis, B.P., Burge, C.B. & Bartel, D.P. Conserved seed pairing, often flanked by adenosines, indicates that thousands of human genes are microRNA targets. *Cell* **120**, 15–20 (2005).
31. Lewis, B.P., Shih, I.H., Jones-Rhoades, M.W., Bartel, D.P. & Burge, C.B. Prediction of mammalian microRNA targets. *Cell* **115**, 787–798 (2003).
32. John, B. *et al.* Human MicroRNA targets. *PLoS Biol.* **2**, e363 (2004).
33. Krek, A. *et al.* Combinatorial microRNA target predictions. *Nat. Genet.* **37**, 495–500 (2005).